Robust Adaptive Quantum-Limited Super-Resolution Imaging

Tianrui Tan*, Kwan Kit Lee†, Amit Ashok†*, Animesh Datta‡, Boulat A. Bash*†
*Department of Electrical and Computer Engineering, University of Arizona, Tucson AZ 85721
†Wyant College of Optical Sciences, University of Arizona, Tucson AZ 85721
‡Department of Physics, University of Warwick, Coventry CV4 7AL, UK
E-mail:{tantianrui, kklee, ashoka, boulat} @arizona.edu, {Animesh.Datta}@warwick.ac.uk

***Abstract*—Inspired by the results from quantum information processing, spatial-mode demultiplexing offers resolution of objects at the quantum limit, below the well-known Rayleigh-Abbe diffraction limit. An intriguing aspect of these results is that, while the analysis leading to the ultimate sub-diffraction limit is quantum, semi-classical devices can be used to build "super-resolving" sensors that achieve this limit. Therefore, these developments have potential to significantly improve the quality of imaging systems in the near term. However, these quantum-inspired systems are sensitive to fluctuation in nuisance parameters, whether they are natural or adversarial. In this paper we analyze the impact of such fluctuations and provide methods to mitigate it. We focus on a problem of resolving two point sources, which has immediate practical applications in, e.g., space situation awareness.**

I. Introduction

Imaging systems operating in the far field are often understood to have a "fundamental" limit on the optical resolution due to diffraction. Consider a problem of resolving two weak incoherent monochromatic point sources (e.g., two distant stars or two small cellular features). "Rayleigh-Abbe criterion" [1], [2] (or "Rayleigh criterion") describes the minimum angular separation between these sources that can be accurately estimated using a reasonable number of observations. It is a function of the wavelength λ of the detected light and the numerical aperture of the imaging system (which, for distant objects, can be approximated using the diameter of the entrance pupil) [4]. However, this limit implicitly assumes "direct detection" imaging, that is, intensity measurement of the optical image on the focal (image) plane.

It has long been known that more information about the scene can be extracted from the incident optical wavefront by considering other measurement instruments [5, Chapter 30, Footnote 2]. In the last few years, quantum estimation theory [6] has shown mathematically that the diffraction limit is not fundamental, and is an artifact of choosing the direct detection measurement. In fact, it disappears when spatial-mode resolving measurements such as "spatial mode demultiplexing" (SPADE) [7], [8].

SPADE requires precise alignment to the centroid of the scene. Existing solutions estimate the centroid assuming that it is static [9]. In this paper, we study the impact of scene dynamics, focusing on random perturbations of the scene centroid. We find that perturbations increase the mean squared error (MSE) of SPADE's source separation estimate, as do other types of noise [10], [11]. Although we offer a partial correction for the errors introduced by the perturbations, we note that SPADE is surprisingly robust: unless perturbations are extreme, it outperforms direct detection even without our correction! That being said, our study motivates investigating alternative measurements that further improve on SPADE's performance in dynamic regimes.

In the next section, we present the mathematical details of the two-source separation problem and the quantum-inspired approach that enables resolving these sources beyond the Rayleigh-Abbe limit. In Section III we explore the impact of scene dynamics analytically and via Monte Carlo simulation, and in Section IV we conclude.

II. Preliminaries

A. Angular Resolution of Two Point Sources

Consider the problem of estimating the angular separation s between the two equal-relative-brightness point sources in a single dimension, as depicted in Fig. 1(a). The radiant emittance of the two point sources is described mathematically using two Dirac delta functions:

$$r(y;s,c)=\frac{1}{2}\left[\delta\left(y-y_0\right)+\delta\left(y-y_1\right)\right], \tag{1}$$

where

$$y_0=c+s/2, \qquad y_1=c-s/2, \tag{2}$$

c is the spatial centroid of the imaging system, and y is the object plane coordinate [4, Ch. 7]. In the far-field diffraction-limited regime, the point spread function (PSF) $\psi(x)$ is the Fourier transform of the aperture function. The spatial distribution of energy in the image plane is the convolution of the object radiant emittance function and $|\psi(x)|^2$:

$$I(x;s,c)=\int_{-\infty}^{+\infty} r(y;s,c)|\psi(x-y)|^2\,dy, \tag{3}$$

where x is the image plane coordinate scaled with respect to the magnification factor of the imaging system [4, Ch. 7]. $I(x;s,c)$ can also be interpreted as the probability density function of measuring a photon at position x [4, Ch. 8].

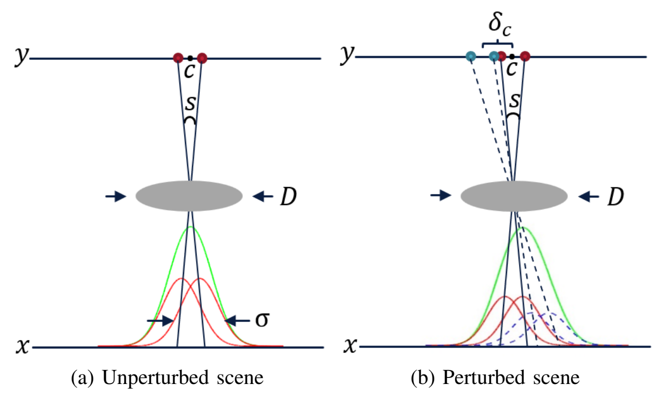

Fig. 1: Resolution of two incoherent monochromatic objects with separation s and centroid c imaged through a Gaussian aperture with diameter D. In Fig. 1(b), the centroid is perturbed randomly by δ_c. We sketch the resulting image plane energy distributions, and show their Gaussian components.

We assume an apodized Gaussian aperture to reduce the diffraction patterns around the intensity peaks, with PSF [12]:

$$\psi(x) = \left(\frac{1}{2\pi\sigma^2}\right)^{\frac{1}{4}} \exp\left(\frac{-x^2}{4\sigma^2}\right). \tag{4}$$

We expect the results that follow to not change significantly for the more practical circular apertures [13]. For distant objects, the width of the PSF σ can be approximated by $\sigma \approx \frac{\lambda}{D}$, where D is the diameter of the 1-D Gaussian aperture of the imaging system and λ is the source center wavelength. Combining (1), (3), and (4), we obtain:

$$I(x; s, c) = \frac{1}{2\sqrt{2\pi\sigma^2}}\left[e^{-\frac{(x-y_0)^2}{2\sigma^2}} + e^{-\frac{(x-y_1)^2}{2\sigma^2}}\right], \tag{5}$$

where y_i is the location of the i^{th} point source defined in (2).

For a lossless, passive, and monochromatic imaging system employing direct detection measurement (photo-detection), the Cramér-Rao bound on the MSE of any unbiased estimator $\check{s}$ of the angular separation s is [14]–[16]:

$$\text{MSE}(\check{s}) \geq \frac{1}{NH(s)}, \tag{6}$$

where N is the total mean photon number and $H(s)$ is the Fisher information (FI) per photon [7], [13]:

$$H(s) = \int_{-\infty}^{+\infty} \frac{1}{I(x; s, c)}\left(\frac{\partial I(x; s, c)}{\partial s}\right)^2 dx. \tag{7}$$

The well-known Rayleigh-Abbe criterion describes the limit of resolving two spatially incoherent sources. Specifically, it states that the MSE of estimating separation s substantially increases when s falls below $\sim \frac{\lambda}{D}$, necessitating more observations to resolve the objects. Since MSE is proportional to σ^2 and is inversely proportional to N, we consider the normalized MSE$\times N/(4\sigma^2)$. The corresponding CRB is similarly normalized. Fig. 2 illustrates the degradation of performance by showing that the normalized CRB for the MSE of direct detection increases substantially as the normalized separation $\frac{s}{\sigma}$ tends to zero [14], [17].

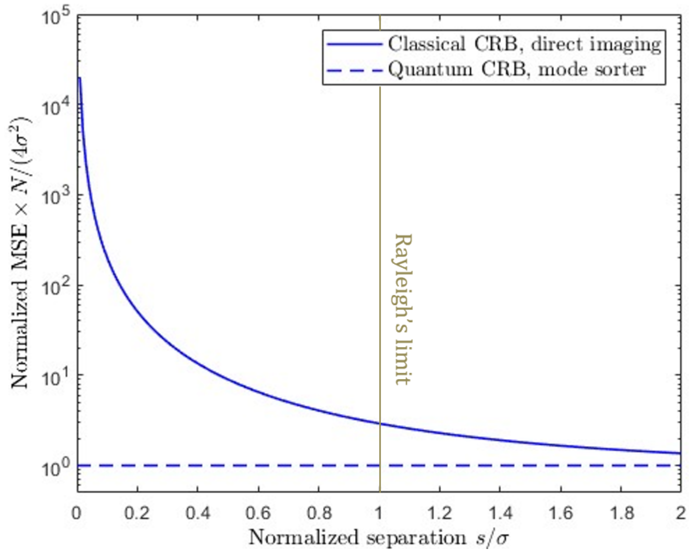

Fig. 2: Normalized CRB for the MSE of estimating separation s vs. normalized separation s/σ showing the performance limits for direct imaging and mode-sorting measurements.

B. *Quantum-inspired Super-resolution*

Despite the fact that here we only consider classical light, quantum information processing provides insights to reach beyond the Rayleigh-Abbe limit. We can describe the quantum state of a photon from source $i \in \{0, 1\}$ after exiting the aperture using a pure state with the Gaussian PSF:

$$\begin{aligned} |\psi(y_i)\rangle &= \int dx\, \psi(x - y_i)\, |x\rangle \\ &= \frac{1}{(2\pi\sigma^2)^{\frac{1}{4}}} \int dx\, e^{-\frac{(x-y_i)^2}{4\sigma^2}}\, |x\rangle\,, \end{aligned} \tag{8}$$

where y_i is the location of the i^{th} point source defined in (2) and $|x\rangle$ is the image plane spatial basis. Therefore, the density operator describing the quantum state (wave-function) of a photon on the image plane is a mixed state:

$$\hat{\rho}(s) = \frac{1}{2}\sum_{i=0,1} |\psi(y_i)\rangle \langle\psi(y_i)|\,. \tag{9}$$

In order to estimate s, one must measure the quantum state $\hat{\rho}(s)$. Quantum mechanics allows for a rich choice of measurements, with direct detection being one of the choices. The ultimate quantum limit on the MSE is the quantum CRB [6], which optimizes the classical CRB over all the possible quantum measurements:

$$\text{MSE}(\check{s}) \geq \frac{1}{NH(s)} \geq \frac{1}{NQ(s)}, \tag{10}$$

where $Q(s)$ is the quantum FI [6]:

$$Q(s) = \text{Tr}\left[\hat{\rho}(s)\hat{L}_s^2\right]. \tag{11}$$

Here $\hat{L}_s$ is the symmetric logarithmic derivative (SLD) [18] with respect to the angular separation s, represented implicitly by the Lyapunov equation [19]:

$$\frac{\partial \hat{\rho}(s)}{\partial s} = \frac{1}{2}(\hat{L}_s \hat{\rho}(s) + \hat{\rho}(s)\hat{L}_s). \tag{12}$$

As seen in Fig. 2, quantum CRB does not degrade with s. Thus, Rayleigh-Abbe limit is not fundamental and is entirely due to the choice of direct detection measurement. Resolution of objects beyond Rayleigh-Abbe limit, or *super-resolution* is, therefore, possible with another measurement.

A measurement that projects the wave-function $\hat{\rho}(s)$ of the photon on the image plane into spatial Hermite-Gaussian (HG) mode basis $\{|\phi_q\rangle \langle\phi_q|\}$, $q = 0, 1, \ldots$, and directly detects the photons on each mode saturates the second inequity of (10) [7]. The HG modes are orthonormal and are given by:

$$|\phi_q\rangle = \left(\frac{1}{2\pi\sigma^2}\right)^{\frac{1}{4}} \frac{1}{\sqrt{2^q q!}} \int dx\, H_q\!\left(\frac{x}{\sqrt{2}\sigma}\right) e^{-\frac{x^2}{4\sigma^2}} |x\rangle, \tag{13}$$

where $H_q(x)$ is a polynomial – an eigenfunction of the Gaussian function. This spatial mode projection followed by photo-detection is called <u>s</u>*patial* *mode* <u>de</u>*multiplexing* or SPADE. In fact, a projection into a binary spatial mode set $\{|\phi_0\rangle \langle\phi_0|, I - |\phi_0\rangle \langle\phi_0|\}$ followed by photo-detection on each of the two modes (called B-SPADE) also saturates the quantum limit in (10) [7], [9]. We will thus analyze B-SPADE in the remainder of the paper.

C. Two-stage B-SPADE Receiver

Knowledge of the centroid value c is necessary to align the spatial mode projection to the scene. An adaptive two-stage approach depicted in Fig. 3 was proposed in [9]. In the first stage N_1 photons are directly-detected. Then, the positions of photon detection are averaged, producing an unbiased estimator $\hat{c}$. It is used to construct B-SPADE in the second stage to estimate separation s using the remaining $N_2 = N - N_1$ photons. Maximum likelihood estimation (MLE) employed on the output of the detectors yields an asymptotically consistent estimator of s that achieves quantum CRB as $N \to \infty$. In [9], the authors optimize N_1. We employ a simplification inspired by [20, Ch. 6], [21], [22] and set $N_1 = \sqrt{N}$. This simplified adaptive multistage imaging system saturates the quantum CRB in (10) for large N.

III. Impact of Scene Dynamics

A. Random Centroid Perturbations

Authors of [9] assume that the scene is static. In particular, while the centroid is unknown, it is assumed not to move as measurements are performed. However, in many practical scenarios, the centroid location changes randomly, e.g., due to the vibration of the sensing platform. Here we explore the impact of the centroid perturbations on resolving the two incoherent point sources. We employ a simplified model of centroid dynamics: each photon arrives independently with probability $1 - p$ from an unperturbed scene with unknown centroid c and with probability p from a centroid moved to

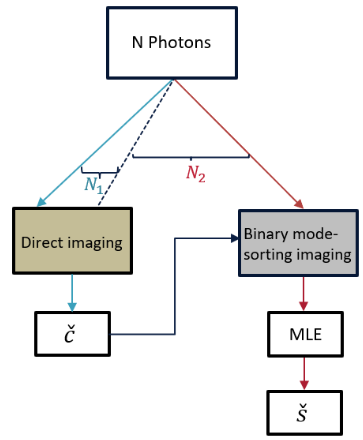

Fig. 3: Two-stage receiver design. We set $N_1 = \sqrt{N}$ and $N_2 = N - \sqrt{N}$.

$c + \delta_c$, for $\delta_c > 0$. This is described in Fig. 1(b). The spatial distribution of energy on the image plane from the perturbed scene is:

$$I_{\mathrm{p}}(x; s, c, p, \delta_c) = (1 - p)I(x; s, c) + pI(x; s, c + \delta_c), \tag{14}$$

where $I(x; s, c)$ is defined in (5) and subscript "p" denotes "perturbed." The corresponding quantum state of a photon is:

$$\begin{aligned}\hat{\rho}_{\mathrm{p}}(s) = &\frac{1}{2}(1-p) \sum_{i=0,1} |\psi(y_i)\rangle \langle\psi(y_i)| \\ &+ \frac{1}{2}p \sum_{i=0',1'} |\psi(y_i')\rangle \langle\psi(y_i')|,\end{aligned} \tag{15}$$

where

$$y_0' = (c + \delta_c) + s/2, \qquad y_1' = (c - \delta_c) - s/2. \tag{16}$$

Consider using the two-stage imaging system from [9] as described in Section II-C without adjusting for centroid dynamics. Then, the perturbations degrade resolution by 1) introducing bias into the estimate of centroid location $\hat{c}$, and 2) causing misalignment of the mode sorter. Suppose both p and δ_c are known (e.g., from the understanding of the underlying physical properties of the system). Then, the naïve centroid estimator $\hat{c}$ described in Section II-C can be corrected to return the unperturbed value in expectation as follows:

$$\check{c}_u = \check{c} - p\delta_c. \tag{17}$$

Although this is a partial solution, it ameliorates the performance degradation due to perturbations, as we show in our numerical study that follows.

B. Numerical Results

We employ Monte-Carlo simulations to study the impact of centroid perturbations. We simulate the estimation of angular separation s using the direct-detection imaging, the naïve two-stage B-SPADE measurements, and the two-stage B-SPADE

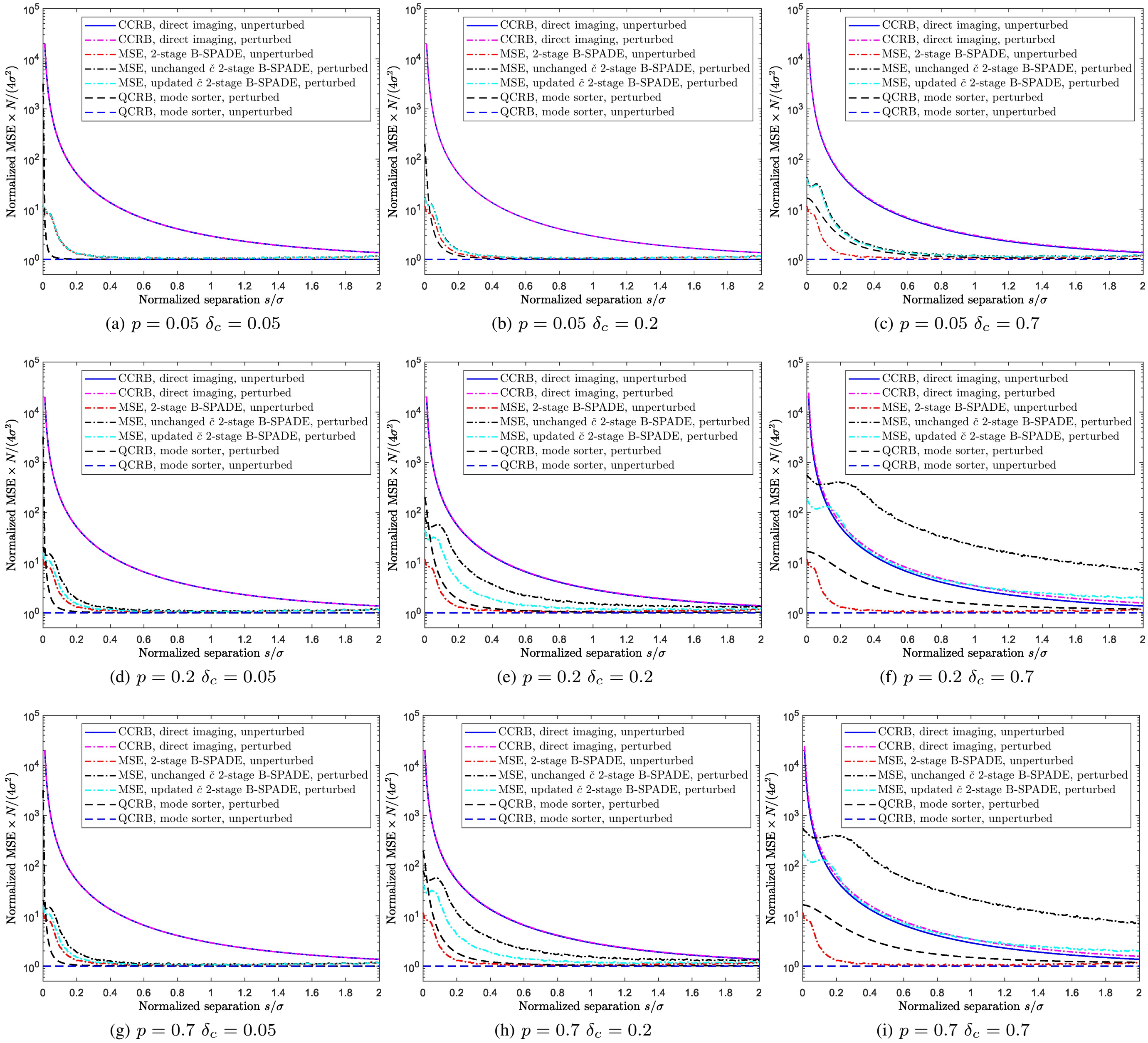

(a) $p = 0.05$ $\delta_c = 0.05$ (b) $p = 0.05$ $\delta_c = 0.2$ (c) $p = 0.05$ $\delta_c = 0.7$

(d) $p = 0.2$ $\delta_c = 0.05$ (e) $p = 0.2$ $\delta_c = 0.2$ (f) $p = 0.2$ $\delta_c = 0.7$

(g) $p = 0.7$ $\delta_c = 0.05$ (h) $p = 0.7$ $\delta_c = 0.2$ (i) $p = 0.7$ $\delta_c = 0.7$

Fig. 4: Normalized MSE of estimating separation s vs. normalized separation s/σ. The total mean photon number is $N = 10^5$. CCRB and QCRB are normalized classical and quantum Cramér-Rao bounds. We evaluate the MSE at 201 equally-spaced values of $s/\sigma \in [0, 2]$. Each data point is an average of $n = 5\times10^3$ results from Monte-Carlo simulations. The 95% confidence intervals are negligibly small and not reported.

with perturbation bias removed from the estimator $\check{c}$ of the centroid location c using (17). These are described in Sections II-A, II-C, and III-A, respectively. We also evaluate the corresponding classical and quantum CRBs. Our total mean photon number is $N = 10^5$ and we average over the results of $n = 5\times10^3$ Monte-Carlo simulation trials to obtain each data point. Both n and N are limited by our computing capabilities. Recall that the MLE used on the output of photodetectors that follow the mode sorters are inherently biased at finite N. Thus, while increasing n would not change our results significantly (our 95% confidence intervals are negligible), increasing N would be beneficial.[1] Our perturbation parameters are $p \in \{0.05, 0.2, 0.7\}$ and $\delta_c \in \{0.05, 0.2, 0.7\}$. We normalize MSE and CRB via multiplication by $N/(4\sigma^2)$ as described in Section II-A.

[1]The "humps" in the MSE curves, such as those found for the MSEs in both naïve and updated receivers for $p = 0.2$ and $\delta_c = 0.7$ around $s/\sigma \approx 1.5$ in Fig. 4(f) are due to the MLE bias. We expect larger N to reduce their size.

The plots on Fig. 4 reveal that the bias in centroid estimation as well as the misalignment of the mode sorter increases the MSE for B-SPADE measurement. However, B-SPADE still outperforms direct detection for all except very large centroid perturbations in Fig. 4(i)! Furthermore, the bias correction in (17) decreases MSE substantially, although it does not achieve the quantum CRB. Additionally:

- The effect of even large centroid perturbations in Fig. 4(i) on the direct detection imaging is insignificant.
- On the other hand, centroid perturbations increase the quantum CRB for resolution MSE substantially. This is especially noticeable at small s and δ_c, when the perturbations introduce false excitations that are indistinguishable from the ground truth. Qualitatively similar results hold when mode sorting is afflicted with intermodal cross-talk [10] and thermal noise [11].
- However, when δ_c gets large, the quantum CRB for resolution MSE decreases. This is evident from comparing Figs. 4(a), 4(d), and 4(g) to Figs. 4(c), 4(f), and 4(i). We conjecture that this is because, when δ_c is large, the perturbation component $I(x; s, c + \delta_c)$ of the spatial distribution of energy $I_{\mathrm{p}}(x; s, c, p, \delta_c)$ given in (14) can be distinguished from the ground truth $I(x; s, c)$.

Finally, we note that, although centroid perturbations can severely degrade the performance of B-SPADE, it still uniformly outperforms direct detection in all but the most severe perturbation scenario in Fig. 4(i). However, reaching quantum CRB is likely to require a more complicated design.

IV. Conclusion

Although we show that B-SPADE is surprisingly robust to centroid perturbations, this paper motivates the development of the measurements that achieve the quantum CRB in the perturbed scenario. Incorporation of scene dynamics is also a natural extension of the adaptive Bayesian super-resolution imaging [23]. Furthermore, we assumed full knowledge of the statistical characteristics of perturbations, which is generally unavailable in practice. Receivers that include the estimation of these characteristics need to devised. Finally, the perturbation model needs to be expanded to account for richer set of scene dynamics and include variation in angular separation in addition to centroid.

References

[1] E. Abbe, "Beiträge zur theorie des mikroskops und der mikroskopischen wahrnehmung," *Archiv für Mikroskopische Anatomie*, vol. 9, no. 1, pp. 413–468, Dec. 1873, english translation in [3].

[2] L. Rayleigh, "Investigations in optics, with special reference to the spectroscope," *Philos. Mag.*, vol. 8, pp. 261–274, May 1879.

[3] E. Abbe, "Contributions to the theory of the microscope and the nature of microscopic vision," in *Selected papers on resolution enhancement techniques in optical lithography*, ser. Resolution enhancement techniques in optical lithography, F. M. Schellenberg, Ed. Bellingham, WA, USA: SPIE Press, 2004, pp. 12–24, translation of.

[4] J. Goodman, *Introduction to Fourier Optics*. W. H. Freeman, 2017.

[5] R. Feynman, R. Leighton, M. Sands, and E. Hafner, *The Feynman Lectures on Physics; Vol. I.* Available at https://www.feynmanlectures.caltech.edu. California Institute of Technology, 2013. [Online]. Available: https://www.feynmanlectures.caltech.edu

[6] C. W. Helstrom, *Quantum Detection and Estimation Theory*. New York, NY, USA: Academic Press, Inc., 1976.

[7] M. Tsang, R. Nair, and X.-M. Lu, "Quantum theory of superresolution for two incoherent optical point sources," *Phys. Rev. X*, vol. 6, p. 031033, Aug. 2016.

[8] M. Tsang, "Resolving starlight: a quantum perspective," *Contemp. Phys.*, vol. 60, no. 4, pp. 279–298, 2019.

[9] M. R. Grace, Z. Dutton, A. Ashok, and S. Guha, "Approaching quantum-limited imaging resolution without prior knowledge of the object location," *J. Opt. Soc. Am. A*, vol. 37, no. 8, pp. 1288–1299, Aug. 2020.

[10] M. Gessner, C. Fabre, and N. Treps, "Superresolution limits from measurement crosstalk," *Phys. Rev. Lett.*, vol. 125, p. 100501, Aug. 2020.

[11] C. Oh, S. Zhou, Y. Wong, and L. Jiang, "Quantum limits of superresolution in a noisy environment," *Phys. Rev. Lett.*, vol. 126, p. 120502, Mar. 2021.

[12] G. E. S. Gerald F. Marshall, *Handbook of Optical and Laser Scanning*, 2nd ed. CRC Press, 2012.

[13] R. Kerviche, S. Guha, and A. Ashok, "Fundamental limit of resolving two point sources limited by an arbitrary point spread function," in *Proc. IEEE Int. Symp. Inform. Theory (ISIT)*, Aachen, Germany, Jun. 2017, arXiv:1701.04913 [physics.optics].

[14] S. Ram, E. S. Ward, and R. J. Ober, "Beyond rayleigh's criterion: a resolution measure with application to single-molecule microscopy," *Proceedings of the National Academy of Sciences*, vol. 103, no. 12, pp. 4457–4462, 2006.

[15] R. J. Ober, S. Ram, and E. S. Ward, "Localization accuracy in single-molecule microscopy," *Biophys. J.*, vol. 86, no. 2, pp. 1185–1200, 2004.

[16] J. Chao, E. S. Ward, and R. J. Ober, "Fisher information theory for parameter estimation in single molecule microscopy: tutorial," *J. Opt. Soc. Am. A*, vol. 33, no. 7, pp. B36–B57, Jul. 2016.

[17] E. Bettens, D. Van Dyck, A. Den Dekker, J. Sijbers, and A. Van den Bos, "Model-based two-object resolution from observations having counting statistics," *Ultramicroscopy*, vol. 77, no. 1-2, pp. 37–48, 1999.

[18] M. G. A. Paris, "Quantum estimation for quantum technology," *Int. J. Quant. Inf.*, vol. 7, no. supp01, pp. 125–137, 2009.

[19] J. Liu, J. Chen, X.-X. Jing, and X. Wang, "Quantum fisher information and symmetric logarithmic derivative via anti-commutators," *J. Phys. A: Math. Theor.*, vol. 49, no. 27, p. 275302, 2016.

[20] M. Hayashi, *Quantum Information Theory: Mathematical Foundation*. Springer-Verlag Berlin Heidelberg, 2017.

[21] R. D. Gill and S. Massar, "State estimation for large ensembles," *Phys. Rev. A*, vol. 61, p. 042312, Mar. 2000.

[22] M. Hayashi and K. Matsumoto, "Statistical model with measurement degree of freedom and quantum physics," in *Asymptotic Theory of Quantum Statistical Inference: Selected Papers*, M. Hayashi, Ed. Singapore: World Scientific Publishing Co. Pte. Ltd., 2005, pp. 162–169.

[23] K. K. Lee, C. N. Gagatsos, S. Guha, and A. Ashok, "Quantum-inspired multi-parameter adaptive bayesian estimation for sensing and imaging," *IEEE J. Sel. Topics Signal Process.*, 2022.